LANGMUIR

pubs.acs.org/Langmuir Article

Evaluating the Exfoliation Efficiency of Quasi-2D Metal Diboride Nanosheets Using Hansen Solubility Parameters

Matthew S. Gilliam, Ahmed Yousaf, Yuqi Guo, Duo O. Li, AbdulAziz Momenah, Qing Hua Wang, and Alexander A. Green*



Cite This: Langmuir 2021, 37, 1194-1205



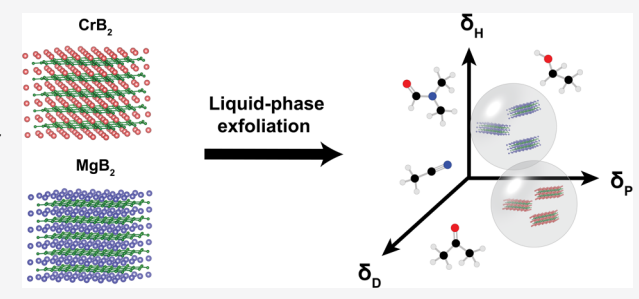
ACCESS

III Metrics & More

Article Recommendations

3 Supporting Information

ABSTRACT: Non-van der Waals (non-vdW) solids are emerging sources of two-dimensional (2D) nanosheets that can be produced via liquid-phase exfoliation (LPE), and are beginning to expand our understanding of 2D and quasi-2D materials. Recently, nanosheets formed by LPE processing of bulk metal diborides, a diverse family of layered non-vdW ceramic materials, have been reported. However, detailed knowledge of the exfoliation efficiency of these nanomaterials is lacking, and is important for their effective solution-phase processing and for understanding their fundamental surface chemistry, since they have significant differences from more conventional nanosheets produced from layered vdW compounds.



Here in this paper we use Hansen solubility theory to investigate nanosheets of the metal borides CrB_2 and MgB_2 derived from LPE. By preparing dispersions in 33 different solvents, we determine Hansen solubility parameters (δ_D , δ_P , δ_H) for both these metal diborides. We find that they exhibit notably higher δ_P and δ_H values compared to conventional vdW materials such as graphene and MoS_2 , likely as a result of the types of bonds broken in such materials from exfoliation which allows for more favorable interactions with more polar and hydrogen-bonding solvents. We apply the solubility parameters to identify cosolvent blends suitable for CrB_2 and MgB_2 that produce dispersions with concentrations that match or exceed those of the top-performing individual solvents for each material and that have markedly higher stability compared to the constituent solvents of the blends alone. This work provides insight into the exfoliation effectiveness of different solvents for preparation of nanosheets from metal diborides and non-vdW materials in general. Such knowledge will be crucial for developing liquid-phase exfoliation strategies for incorporating these materials in applications such as nanocomposites, inks, and coatings.

■ INTRODUCTION

Two-dimensional (2D) nanosheets prepared by liquid-phase exfoliation (LPE) have been extensively studied due to their ease of synthesis, solution-phase processability, and excellent materials properties. Many well-known 2D nanomaterials prepared by LPE,1 such as graphene, transition metal dichalcogenides (TMDCs), and hexagonal boron nitride (hBN), have been used in applications including printable electronics, polymer nanocomposites, and solution-phase catalysis.^{2–4} Most 2D nanosheets are generated from parent materials that have layered bulk crystal structures consisting of sheets held together by van der Waals (vdW) forces that are readily separated. Extensive work has been done in not only applying the exceptional properties of vdW 2D nanomaterials in the solution phase, but also in optimizing nanosheet concentration, thickness selectivity, and diversity of available dispersing media. 5-7 In recent years quasi-2D nanosheets have been prepared from materials that lack a layered vdW parent structure, expanding the study of 2D exfoliation to a diverse assortment of new materials. For example, the non-vdW natural ore minerals hematite and ilmenite have been

successfully prepared using LPE and combined with titania nanotubes to construct photocatalytic devices. 8,9 Various nonlayered earth-abundant materials have been exfoliated and used as electrocatalysts for the oxygen evolution reaction. 10

Recently, we have shown that a class of non-vdW materials, the metal diborides, can be processed into dispersions of quasi-2D nanosheets by LPE in organic solvents. These materials have the general formula MB₂, where M is a metal and B is boron, and have a layered structure as shown in the schematic in Figure 1a. However, the bonding in the metal diborides has some ionic character, and is stronger than vdW interactions. In our earlier work, we produced metal diboride nanosheets that served as effective fillers in polymer nanocomposites,

Received: October 28, 2020 Revised: December 31, 2020 Published: January 11, 2021





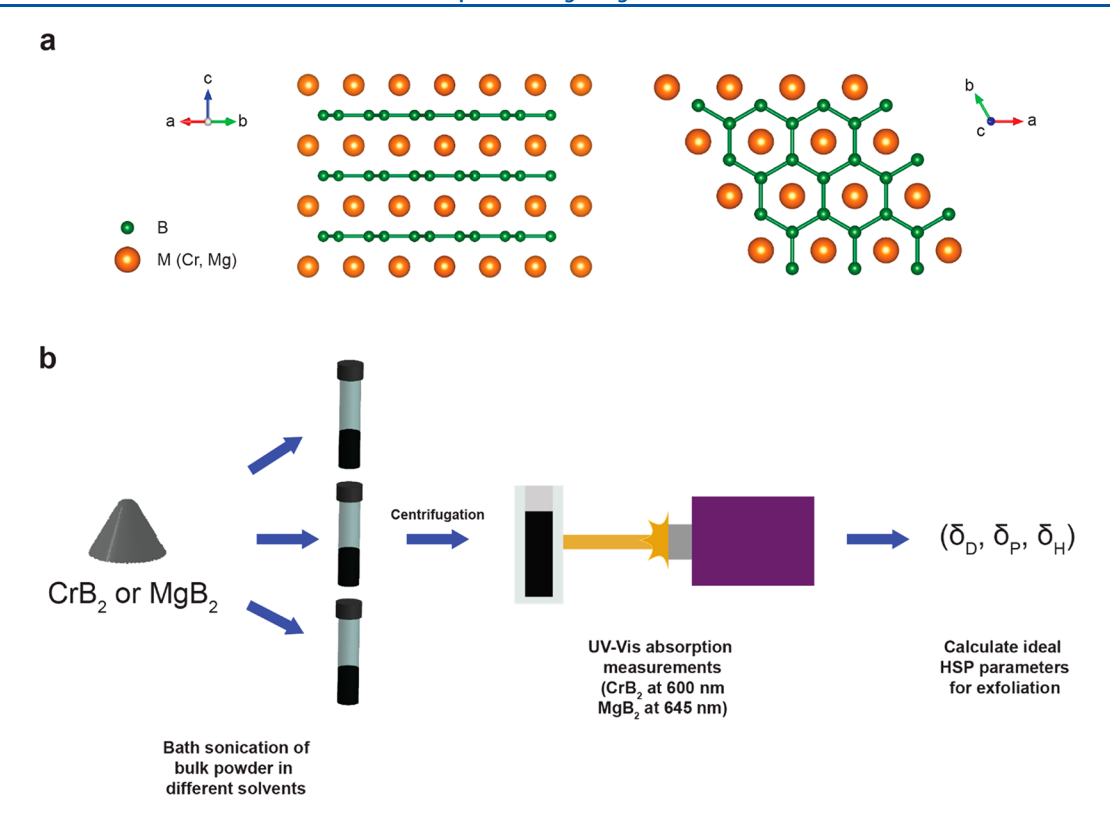


Figure 1. (a) Crystal structure of CrB₂ and MgB₂ showing both lateral (left) and z-axis (right) views. (b) Scheme for conducting solvent study on metal diborides. Dispersions of CrB₂ and MgB₂ are prepared in triplicate by bath sonication and centrifugation of powders in different solvents to remove large aggregates. The concentrations of the dispersions are then measured using UV—vis spectroscopy and the weighted averages of the extinctions and solubility parameters of the solvents are used to estimate HSP values for each material.

demonstrating significant enhancement of the mechanical strength. In addition to mechanical rigidity, some members of the metal diboride family also exhibit bulk properties such as high temperature superconductivity and ultrahigh temperature melting points. They have also been investigated for their catalytic potential in the hydrogen evolution reaction, and more recently a member of the metal diboride family has been shown to demonstrate unique sol—gel chemistry upon reaction with H_2O_2 as well as photocatalytic activity, suggesting many diverse potential uses of their two-dimensional forms.

Since non-vdW materials are held together by stronger covalent, ionic, and metallic bonds instead of comparably weaker vdW interactions, one would expect unique surface interactions with small molecules such as solvents upon exfoliation. For example, because of stronger bonding, it is likely that some surface reconstruction or functionalization would occur to promote stability of the nanosheets against aggregation in a given solvent. Consequently, developing an understanding of how solvents interact with these non-vdW nanosheets and assist in their exfoliation is critical to developing effective solution-phase processing techniques and facilitating their future applications.

However, despite growing interest in LPE nanomaterials derived from non-vdW solids, to our knowledge there have been no extensive experimental reports on the exfoliation behavior of non-vdW structures across various solvents. One way to elucidate the exfoliation behavior of LPE-processed nanosheets is to apply Hansen solubility theory, which assigns three parameters to each solvent to take into account different components of noncovalent intermolecular interactions, based on dispersive $(\delta_{\rm D})$, polar $(\delta_{\rm P})$, and hydrogen-bonding $(\delta_{\rm H})$

interactions.¹⁷ These parameters, called Hansen solubility parameters (HSPs), serve as a means to quantify the "likedissolves-like" concept in solution-phase chemistry, with two species sharing similar HSP values being more likely to mix with each other. In the case of LPE processing of 2D nanomaterials, they can describe the ability of a solvent to effectively stabilize a colloidal dispersion of nanosheets. Previous work has demonstrated that values for the three Hansen parameters can be experimentally estimated for 2D nanomaterials like graphene and molybdenum disulfide (MoS₂) by dispersing the materials in a range of different solvents and determining which set of Hansen values gives the most concentrated dispersions of nanosheets. 18,19 However, this analysis has only been performed thus far with vdWderived 2D nanomaterials. Although one study predicted and demonstrated the successful cosolvent exfoliation of titanium diboride (TiB₂) by calculating its surface tension components and comparing them with various solvents, the work still did not directly examine the exfoliation efficiency of the material in a survey of individual solvents.²⁰ Such broad experimental solvent studies are important for understanding fundamental surface interactions that LPE 2D nanomaterials have with their environment during and after exfoliation, and also provide useful predictive abilities for choosing effective solvents to enhance scalability for research and industrial endeavors.

Herein we examine the exfoliation behavior of two representative non-vdW structures from the class of metal diborides—chromium diboride (CrB₂) and magnesium diboride (MgB₂)—and determine all three HSPs for these two nanomaterials after quantifying the effectiveness of their exfoliation in 33 different solvents. To demonstrate the

applicability of the calculated HSPs for optimizing future exfoliation experiments, we use them to choose and evaluate binary cosolvent blends which can enhance the initial concentration of the nanomaterial dispersions as well as prolong their colloidal stability relative to either constituent solvents alone. We expect that our results will help inform exfoliation efforts other classes of 2D and quasi-2D nanomaterials derived from non-vdW solids and provide predictive insight that can assist in utilizing quasi-2D metal diboride nanosheets in new technologies.

METHODS

Materials. Chromium diboride (99% metals basis, ~325 mesh, Alfa Aesar 12570) and magnesium diboride (powder ~100 mesh ≥99% trace metals basis, Sigma-Aldrich 553913) were used as received

Isopropanol (IPA, Sigma, I9030), ethanol (EtOH, Sigma, E7023), acetone (ACT, VWR, BDH1101), quinoline (Sigma, 241571), pyridine (Pyr, Sigma, 270970), 1-methyl-2-pyrrolidinone (NMP, Sigma, 270458), cyclopentanone (CPO, Sigma, W391018), ethyl acetate (EtAc, Sigma, 270989), acetonitrile (ACN, Sigma, 271004), dimethyl sulfoxide (DMSO, Sigma, D8418), N,N-dimethylformamide (DMF, Sigma, 227056), chloroform (CF, Sigma, C2432), methanol (MeOH, Sigma, 34860), N,N-dimethylacetamide (DMAc, Sigma, D137510), dichloromethane (DCM, Sigma, 270997), dimethyl phthalate (DMP, Sigma, W508500), 1,2-dichlorobenzene (DCB, Sigma, 270598), 1,3-dimethyl-3,4,5,6-tetrahydro-2(1H)-pyrimidinone (DMPU, Sigma, 251569), cyclohexanone (CHO, Sigma, 398241), γbutyolactone (GBL, Sigma, B103608), 1,4-dioxane (Sigma, 296309), ethylene glycol, (EtGly, Sigma, 324558), 1-ethyl-2-pyrrolidone (1EP, Sigma, 146358), heptane (Sigma, 246654), hexane (Sigma, 296090), pentane (Sigma, 236705), formamide (FAm, Sigma, F9037), benzonitrile (BN, Sigma, B8959), dibenzyl ether (DBE, Sigma, 33630), benzyl benzoate (BB, Sigma, B6630), benzaldehyde (BA, Sigma, B1334), 1-vinyl-2-pyrrolidinone (1VP, Sigma, V3409) and 1,3dioxolane (Sigma, 184497) were all used as received.

Dispersion of 2D Metal Diboride Nanosheets. Four hundred mg of either CrB₂ or MgB₂ powder were mixed with 6 mL of solvent in 15 mL glass dram vials subjected to bath sonication (Branson CPX2800H) for 1 h. The samples were sonicated in an ice—water bath to maintain a consistent temperature and prevent overheating during sonication. The sonicated mixtures were then placed into 1.75 mL microcentrifuge tubes and centrifuged at 5000 RCF (Eppendorf Centrifuge 5424, FA-45–24–11 rotor). One mL of the supernatant dispersion containing the metal diboride nanosheets was collected from each tube. Since the solvents used had varying viscosities, a set of centrifugation times adjusted for viscosity were determined by eq 1

$$t_{\rm c} = \frac{4\eta_{\rm s}}{2} \tag{1}$$

which calculates a viscosity-corrected centrifugation (t_c) based on the viscosity of each solvent (η_s) in mPa*s at 25 °C, normalized to a standard 4 min centrifugation time for isopropanol (IPA), which has a viscosity of 2 mPa*s. We have found in earlier experiments that dispersions produced in IPA with a 4 min centrifugation time and 5000 RCF speed were effective for many different metal diboride compositions. The calculated t_c values were rounded to the nearest 0.5 min for experiments. For example, a dispersion made with a solvent with a calculated t_c of 3.3 min would be centrifuged for 3.5 min.

For each metal diboride/solvent combination, dispersions were generated under both viscosity-corrected centrifugation conditions as described above and with a standard centrifugation time of 4 min. Thus, half of each sonicated mixture was centrifuged for 5000 RCF for a time determined based on solvent viscosity calculated using eq 1, and the other half was centrifuged at 5000 RCF for 4 min, independent of viscosity. Each metal diboride/solvent dispersion was prepared in triplicate.

The same viscosity correction was applied to solvent blends, though for two solvents with significantly different viscosities, a different viscosity representing that of the blend needed to be determined. The viscosities for the MeOH and DCB blends were calculated by using the Arrhenius equation for a binary mixture, shown in eq 2 below:

$$\ln(\eta_{b}) = x_{1} \ln(\eta_{1}) + x_{2} \ln(\eta_{2}) \tag{2}$$

where η_b is the viscosity of the solvent blend, η_1 and η_2 are the viscosities of the two pure solvents, and x_1 and x_2 are the solvents' respective mole fractions.

Extinction and Concentration Measurements. Extinction measurements were performed using ultraviolet—visible-near-infrared (UV—vis-NIR) spectroscopy. Spectra for the metal diboride dispersions in quartz cuvettes were collected using a Jasco V-670 spectrophotometer. The extinction values at 600 nm for CrB_2 and at 645 nm for MgB_2 , wavelengths at which the spectra are featureless, were used to calculate the HSP values for each metal diboride. The average extinctions from the triplicate measurements of each dispersion were then used to calculate the Hansen solubility parameters (δ_i) using eq 3.

$$\langle \delta_i \rangle = \frac{\sum_s c_s \delta_{i,s}}{\sum_s c_s} \tag{3}$$

where c_s represents the average extinction of a dispersion of nanosheets in a particular solvent and $(\delta_{i,s})$ is the Hansen solubility parameter value for the particular solvent s, and i is D, P, or H.

Concentration measurements used for calculating the extinction coefficients for CrB₂ and MgB₂ in select solvents were determined using inductively coupled plasma mass spectrometry (ICP-MS). Concentrations of chromium and magnesium were collected using a Thermo Fisher iCap Q Quadrupole instrument. Samples were acidified overnight with HNO₃ and diluted to form an aqueous solution of 2 wt % HNO₃ before being analyzed by the instrument. Because the instrument is not able to measure boron quantitatively enough for concentration determination, concentrations in mg/mL for each metal diboride were inferred from the metal concentrations by assuming stoichiometric amounts of boron were present, and adding that to the metal concentration.

Transmission Electron Microscopy (TEM) and Atomic Force Microscopy (AFM). Samples for TEM analysis were prepared by drop casting CrB_2 and MgB_2 dispersions onto lacey carbon grids. Imaging was performed using a Philips CM-12 TEM under an accelerating voltage of 80 kV.

AFM samples were prepared by spin coating dispersions onto ${\rm SiO_2/Si}$ substrates. The substrates were first cleaned in ACT and IPA prior to spin-coating, and after spin-coating the substrates were annealed in a tube furnace at 400 °C with flowing argon to remove any residual organic solvent or other contamination. AFM imaging was performed with a Bruker Multimode V instrument in ScanAsyst noncontact mode with ScanAsyst-Air tips (Bruker, tip diameter 2 nm). Images were processed using Gwyddion software v. 2.52. 22

■ RESULTS AND DISCUSSION

Production and Concentration Measurements of CrB₂ and MgB₂ Nanosheet Dispersions. CrB₂ and MgB₂ belong to a class of metal diborides exhibiting a characteristic layered hexagonal structure, as depicted in Figure 1a. The structures consist of graphene-like boron sheets alternating with layers of metal atoms. In our previous work, we demonstrated the successful exfoliation via LPE of eight different metal diboride compositions into dispersions of 2D nanosheets. In a small survey of six solvents, we found that metal diborides with more ionic bonding character (e.g., MgB₂) tended to exfoliate more effectively than the other compounds. For this study, we decided to focus on two metal diboride compositions, MgB₂ and CrB₂, to more thoroughly

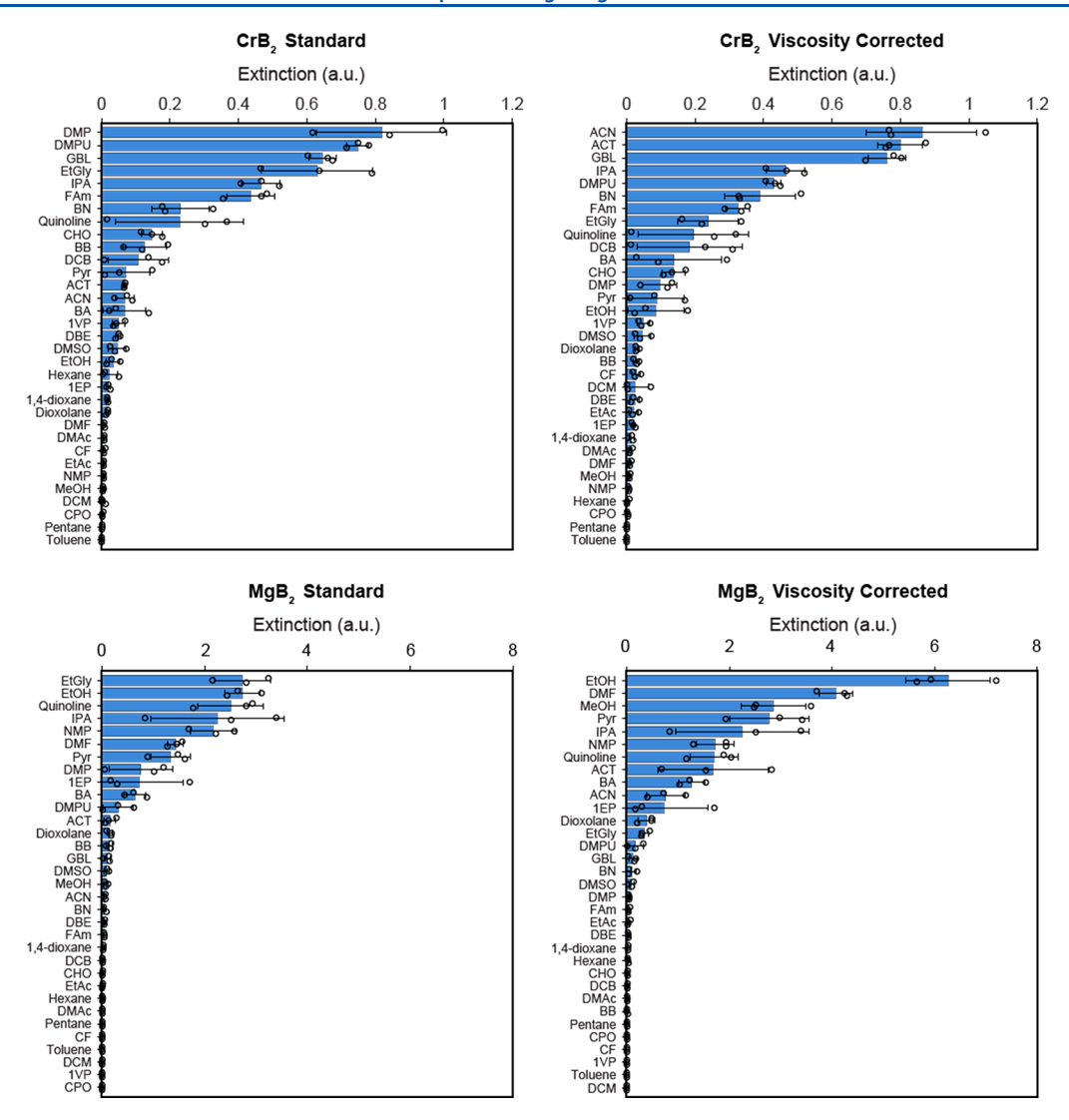


Figure 2. Average extinction measured for CrB_2 and MgB_2 dispersed by different solvents from three trials of measurement for each solvent. Circles represent the data from individual measurements.

characterize their ability to be produced via LPE by determining their HSP values. We chose MgB₂ due to its industrial importance as a potential substitute for current high temperature superconductor-based devices and also due to its relevance in recent research efforts to produce various boron-based 2D nanomaterial compositions via solution-phase chemistry methods.^{23–25} We selected CrB₂ as a less ionic counterpart to MgB₂ and also for its practical use as a nanofiller for polymer nanocomposites, as demonstrated in our previous work.¹¹ We also chose these two metal diborides to provide an example of a compound that exfoliated relatively easily into organic solvents, MgB₂, and contrast it with one that was not easily exfoliated, CrB₂.

Figure 1b depicts the methodology used for determining the exfoliation efficiency of the metal diborides in different solvents. Dispersions of CrB₂ and MgB₂ were prepared by mixing bulk powders with a solvent and subjecting the mixtures to bath sonication for 1 h, followed by centrifugation to remove unexfoliated aggregates and harvesting of the supernatant. The full list of solvents used in this study is included in Supporting Information (SI) Table S1, along with their HSP values and viscosities. Although there have been prior efforts to assess exfoliation efficiency by taking into

account viscosity,26 previous reports discussing the use of solubility parameters to predict nanosheet dispersions neglect the viscosity of the solvent in their processing methods. However, solvent viscosity directly impacts the centrifugation process by reducing the sedimentation velocity of the nanosheets and affecting the concentration of nanosheets that remain in the supernatant following centrifugation. Accordingly, we used viscosity-corrected centrifugation times in this study to compensate for the effect of viscosity in the determination of exfoliation efficacy (see Methods for calculation of viscosity-corrected centrifugation time and SI Table S1 for solvent viscosities and centrifugation times). We note that the viscosity of the solvent can also influence the sonication efficiency, but the power level is not as easily precisely controlled in the bath sonication process and there tends to be some batch-to-batch variation, so we chose to focus on adjusting for the centrifugation time instead, which gave us much more precise control.

The optical extinction of the supernatant was then measured to assess the relative nanosheet concentrations of the dispersions in different solvents. UV—vis-NIR spectra of each material dispersed in their five most effective solvents are shown in SI Figure S1. The dispersions of CrB₂ nanosheets

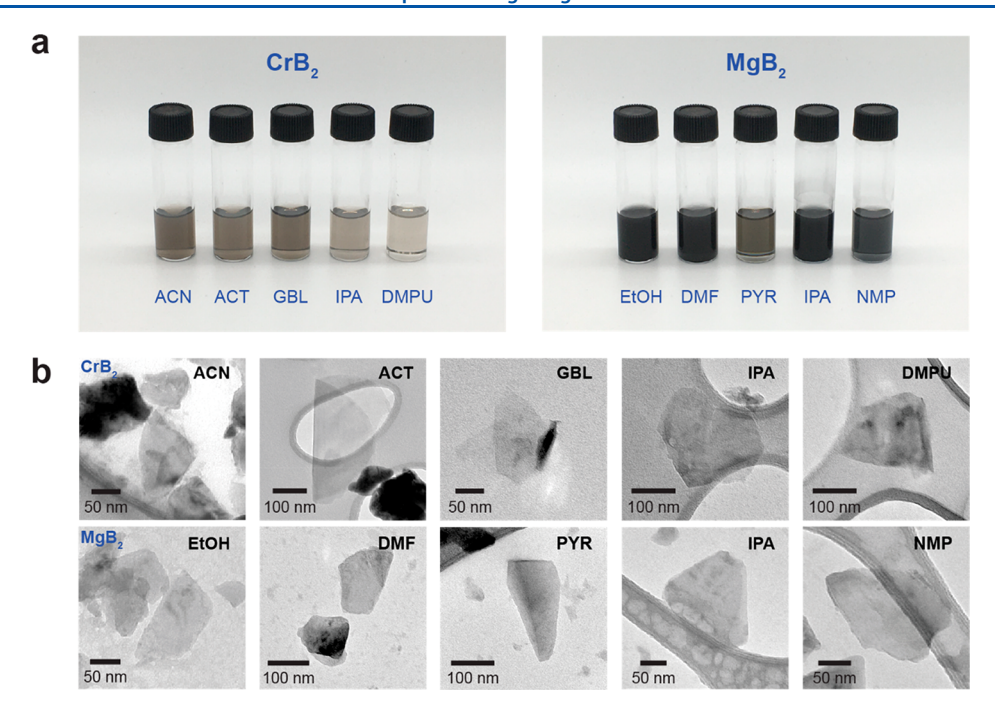


Figure 3. (a) Vials containing the top five most concentrated CrB₂ and MgB₂ dispersions under viscosity-corrected centrifugation conditions. (b) TEM images of CrB₂ and MgB₃ nanosheets contained within the dispersions shown in the above vials.

exhibit relatively featureless spectra, and the extinction of each CrB₂ nanosheet dispersion was evaluated at 600 nm to determine the relative concentration. However, dispersions of MgB₂ nanosheets display two characteristic peaks, one within the range of 410-475 nm and the other within the range of 905-1050 nm. We observed that the peaks in the MgB₂ spectra shift in relative intensity and position depending on the solvent and the centrifugation time used. Since the region between the two peaks at 645 nm was largely unaffected by the two peaks, it was chosen to be the wavelength at which to determine the relative concentration of MgB2 dispersions. The extinction values for the dispersions of both materials are meant to substitute for absolute concentration measurements. To show the linear relationship between the two for the two representative materials, we calculated extinction coefficients for the most effective solvents for both materials. The extinction coefficients and the plots used to calculate them are shown in SI Figure S2. We note that the optical extinction method is used here in our HSP analysis because it allows us to compare to other literature on LPE-derived nanosheets, 4,18,27-30 and allows the colloidally stabilized nanosheets to be measured rather than a compacted surface that would be needed for alternative HSP analysis methods such as those based on contact angle measurements.³¹

Comparison of Dispersion Effectiveness between Solvents. The mean extinction data for both materials under viscosity-corrected centrifugation times and a standard centrifugation time of 4 min are presented in Figure 2 (see SI Tables S2 and S3 for listed extinction values of all dispersions of CrB₂ and MgB₂, respectively). Photographs of vials containing the top five most concentrated dispersions under viscosity-corrected conditions are shown in Figure 3a. We note that there are some batch-to-batch variations, and the optical appearance of these vials are only meant to show the uniform dispersions and not the values of concentrations, which are more accurately represented in the plots in Figure 2. There are some trends in the best solvents for each metal diboride.

Under standard centrifugation conditions, the most effective solvent for dispersing CrB₂ was DMP, which is the most viscous solvent used in the present study. However, when adjusting centrifugation time for viscosity, DMP does not even rank among the top five most effective solvents. The most effective solvent is instead the low-boiling-point solvent ACN, producing samples that range in concentration from 0.010 to 0.022 mg/mL. Additionally, ACT, which like ACN was not present in the top five most effective solvents under standard centrifugation conditions, produced dispersions with comparable concentrations to the top solvent ACN. We found that EtOH is the superior solvent for dispersing MgB₂ nanosheets in this study and can produce dispersions with concentrations of up to 0.502 mg/mL.

Although several of the other top solvents for both MgB₂ and CrB₂ dispersions are common across centrifugation conditions, the exfoliation effectiveness can be overestimated for very viscous solvents (e.g., DMP) and can be underestimated for less viscous solvents (e.g., ACN and ACT). The latter case is particularly noteworthy, as ACN and ACT are low-boiling point solvents that can be valuable for solution-processing applications. Their exceptional ability to exfoliate metal diboride nanosheets would not be as noticeable without taking into account their lower viscosities. Because of the importance of viscosity in LPE experiments, the data obtained under viscosity-corrected conditions will be discussed in the following sections for comparison with other nanomaterials and for predicting and evaluating solvent blends.

Although MeOH was the third best solvent for MgB₂ based on extinction immediately after production, we observed that the initially concentrated dispersion of nanosheets was highly unstable, resulting in irreversible aggregation within only a few hours of exfoliation. Thus, for additional analysis such as TEM, we neglected MeOH in the top five solvent category for MgB₂. We only observed this behavior (i.e., strong initial dispersion followed by rapid aggregation) in MeOH dispersions of MgB₂.

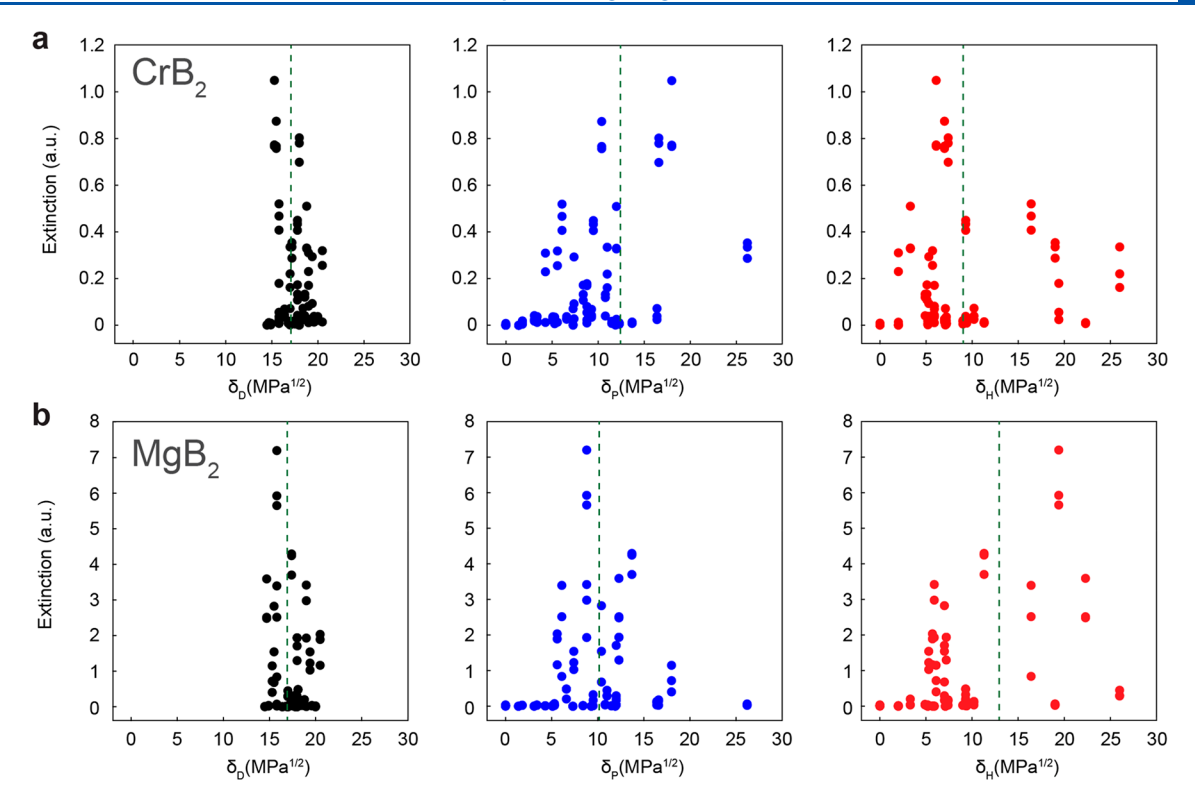


Figure 4. Standard HSP plots depicting the extinction of each metal diboride dispersion plotted against the solubility parameter value of its respective solvent for CrB₂ and MgB₂. Samples of each metal diboride/solvent combination were prepared in triplicate and shown as individual points in plots. Dashed lines represent the calculated HSP value of the metal diboride nanosheets.

We observed the morphology of nanosheets in dispersions produced with the top five most effective solvents by TEM imaging, as shown in Figure 3b. Flake-like nanosheets were observed for all solvent and metal diboride combinations. The areas and thicknesses of CrB2 and MgB2 flakes in their respective top solvents were also analyzed via TEM and AFM analysis, as shown in the histograms in SI Figures S3-S5. Overall, the average areas and thicknesses for each composition are about 2-3 times larger than those of metal diboride nanosheets investigated in our previous work. Such differences are likely due to the fact that tip sonication was used to prepare the dispersions subjected to size and thickness analysis in the previous study, whereas solely bath sonication was used in this work. The weaker forces associated with bath sonication enable the production of larger and thicker flakes than those produced via tip sonication.

Hansen Solubility Parameter Analysis. Figure 4 shows plots of the extinction of the CrB₂ and MgB₂ dispersions versus the HSP values of the solvent. Data from each solvent/metal diboride combination are plotted for all three experimental replicates used for each combination. Using these data, the solubility parameters for CrB₂ and MgB₂ under viscosity-corrected centrifugation conditions were calculated using eq 2. Dashed lines represent the location of the calculated HSP values for CrB₂ and MgB₂ viscosity-corrected conditions. Despite the scatter, for each plot there appears to be a region of HSP values that yields higher extinction, which corresponds to the HSP parameters best for dispersing either CrB₂ or MgB₂ nanosheets.

Figure 5 plots the HSP values for both metal diborides along with previously reported HSP values for other liquid-phase exfoliated 2D nanomaterials including graphene, molybdenum disulfide (MoS₂), germanane, silicane, and a layered double

hydroxide (LDH) Mg₃Al-NO₃. ^{18,19,27-29} For comparison, HSPs for CrB2 and MgB2 under standard centrifugation conditions (i.e., constant 4 min for each solvent) are also included. The exact HSP values for all materials are included in SI Table S4 for reference. We note that the axis ranges for all three HSP values have been chosen to be the same so that they can be more easily compared. From the results in Figure 5, it appears that generally both CrB2 and MgB2 have similarities in HSP values as more traditional 2D nanomaterials such as graphene and MoS₂, particularly in terms of δ_D . However, the values of both δ_P and δ_H are higher in CrB_2 and MgB_2 compared to nanosheets derived from vdW solids. The polar Hansen parameter $\delta_{\rm p}$ describes interactions dictated by dipole moments, and a higher value thus suggests an affinity for more polar solvents. A possible reason for a higher δ_P values for CrB₂ and MgB2 is the presence of oxygen-containing functional groups on the nanosheet surfaces, which are reported to be present in the germanane, silicane, and LDH 2D nanomaterials, whose $\delta_{\rm p}$ values depicted in Figure 5 were also found to be higher than those of graphene and MoS₂. In addition to relatively high $\delta_{\rm P}$ values, CrB₂ and MgB₂ also had quite high $\delta_{\rm H}$ values. Although the Hansen parameter δ_{H} does not strictly represent only the hydrogen-bonding interactions, hydrogen bonding is one of the interactions that can contribute to a high $\delta_{\rm H}$ value. The high $\delta_{\rm H}$ values of hydride-terminated germanane and silicane and the hydroxyl-terminated surfaces of Mg₃Al-NO₃ show the apparent correlation of H-bonding capability and $\delta_{\rm H}$ value, and thus also suggests that the high values of $\delta_{\rm H}$ for CrB2 and MgB2 indicate the presence of H-bonding moieties such as hydroxyl groups on the nanosheet surfaces.

While the δ_P and δ_H values of the two metal diborides are both higher than those of graphene and MoS₂, it is important to note there are also differences that separate the two borides.

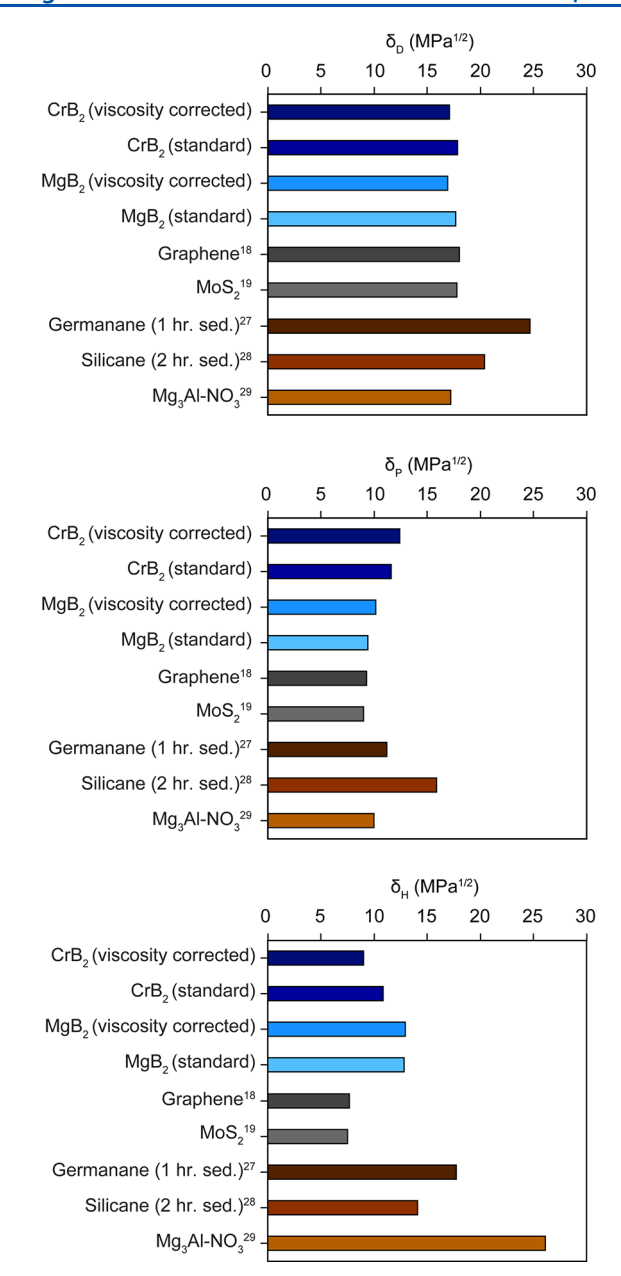


Figure 5. Comparison of HSP values for different nanosheet compositions.

 CrB_2 has a much higher δ_P value than MgB_2 (12.43 for CrB_2 compared to 10.16 for MgB2), while MgB2 has a much higher $\delta_{\rm H}$ value than CrB₂ (12.94 for MgB₂ compared to 9.03 for CrB₂). As MgB₂ exhibits more ionic bonding character than CrB₂, it is reasonable to infer that it would be more easily functionalized with surface hydroxyl groups upon exfoliation, which would lead to a high $\delta_{\rm H}$ value and explain the exceptional exfoliation efficiency of MgB2 in protic solvents like EtOH. Because of the stronger covalent bonding within CrB₂, exfoliation into nanosheets would likely require a greater degree of oxidation of the compound in order for the nanosheets to be stabilized. This behavior would result in the presence of oxygen-containing functional groups on the surface, giving CrB_2 a higher δ_P value and explain the effectiveness of polar aprotic solvents like ACN and ACT in exfoliating CrB₂. Because the CrB₂ and MgB₂ nanosheets are both derived from non-vdW solids, it is likely that the

oxidation of their surfaces with hydroxyl and oxo-functional groups assists in separation of the bulk materials into layers. Thus, the collective functionalization leads to their higher δ_P and δ_H values relative to nanosheets exfoliated from more traditional vdW solids, and higher δ_P and δ_H values could be expected from nanomaterials produced from other non-vdW solids. We note that in our earlier work, we have experimentally detected the presence of boron oxide and boron hydroxide groups, indicating that the boron atomic layers are more likely to be found on the outside of the nanosheets thus leading to some similarities in the HSP values of CrB₂ and MgB₂, but differences in metal—boron bond breaking between CrB₂ and MgB₂ would lead to differences in the polar and hydrogen-bonding values.

Hansen Space Cross Section Plots. The three HSPs of a given solvent or the nanosheets can be thought of as coordinates in a three-dimensional space called the Hansen space. Figure 6 depicts 2D cross sections of Hansen space containing the locations and exfoliation effectiveness of all solvents used in this study along with the calculated coordinates of the CrB2 and MgB2 nanosheets (red filled circles). The mean extinction for each solvent is indicated by its color determined from the color bar, with darker colored points indicating more concentrated dispersions. To aid in the identification of compatible solvents, we defined an ellipse for each cross section centered at the coordinate of the metal diboride. We set the semimajor and semiminor axes of the ellipse to be twice the weighted standard deviation of the calculated HSPs (see SI Equation S1 and Table S5 for the weighted standard deviations). These cross-section plots can also help to visualize the solvents that most contributed to the calculated HSPs of the two nanomaterials, and also help to highlight the overall differences in effective solvents between the two nanomaterials. We note that the axes of all three HSP values have been chosen to be the same, so that the data can be visualized in a scaled 3D Hansen space and more easily

The δ_D - δ_P cross section (Figure 6a) shows that while δ_D varies only slightly between the two materials, $\delta_{\rm p}$ is noticeably higher in CrB_2 , owing to the highly effective solvents with δ_P values greater than 15 that poorly exfoliate MgB2 in comparison. Likewise, for the $\delta_{\rm D}$ - $\delta_{\rm H}$ cross section (Figure 6b), there are more effective solvents with higher $\delta_{\rm H}$ values for MgB₂ than for CrB₂, though it seems possible to exfoliate CrB₂ to at least some extent with solvents possessing a wider range of δ_{H} values. This last point draws attention to a trend that is best illustrated in Figure 6c, which shows the $\delta_{ ext{P}}$ - $\delta_{ ext{H}}$ cross section. While MgB₂ appears to be limited in exfoliation effectiveness to solvents in a δ_P range of 5–15 and a δ_H range of 5-25, CrB2 can still be exfoliated reasonably well with solvents possessing values of both parameters above 25 and below 5. Overall, the greater area encompassed by the ellipse of CrB₂ in each cross section suggests that although CrB₂ cannot be dispersed in high concentrations, it can be exfoliated over a much wider range of solvent properties than MgB2, which might be able to guide further efforts into processing similarly difficult-to-exfoliate materials. For example, even if a non-vdWderived material may not appear to exfoliate well in a solvent that is commonly used in LPE experiments, it does not necessarily mean that a material cannot be exfoliated at all, but rather that the right solvents have not been chosen for that specific material.

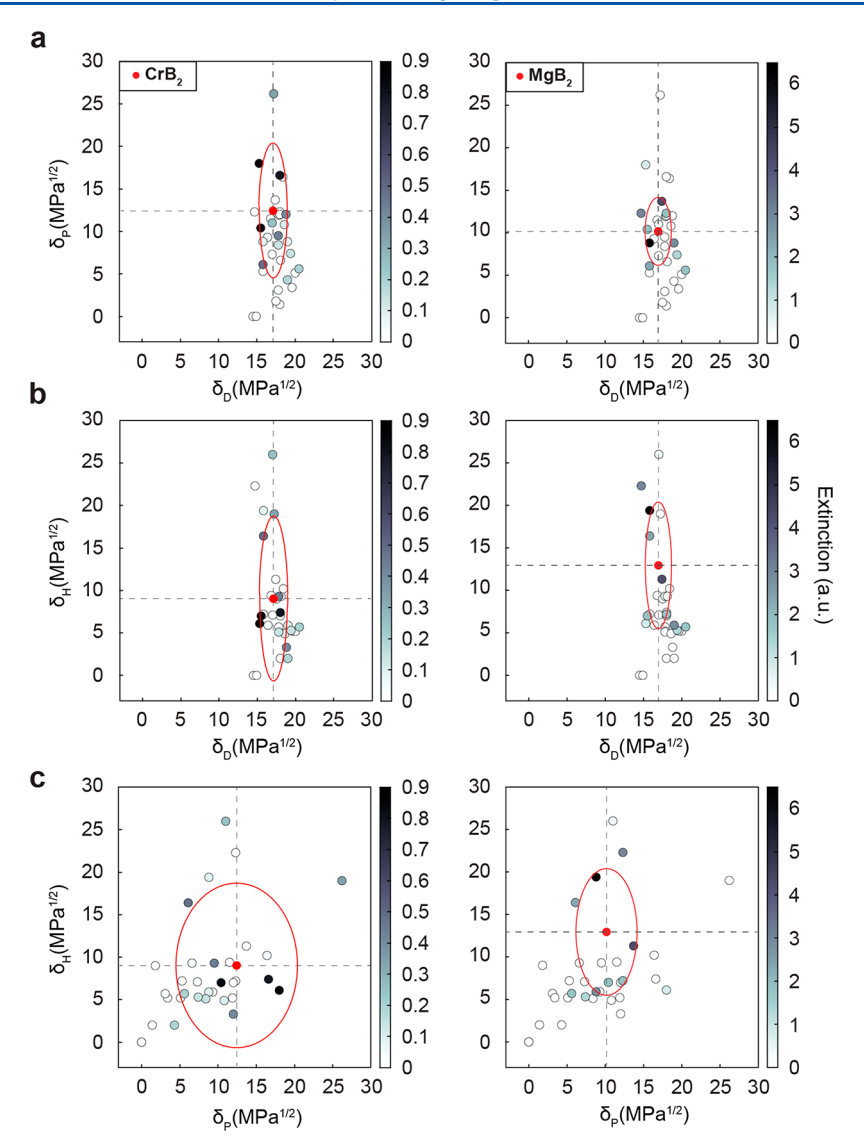


Figure 6. Plots depicting the location in two-dimensional Hansen space for CrB_2 and MgB_2 along with solvents for (a) δ_D - δ_P , (b) δ_D - δ_P , and (c) δ_P - δ_H cross sections. Spots are colored based on the mean extinction of a dispersion produced with each solvent for a given material, with darker-colored spots indicating solvents that produced higher concentrations. The red ellipses are centered at the metal diboride HSPs values and have semimajor and semiminor axes set at twice the weighted standard deviation of the HSPs. They define in Hansen space the HSPs for solvents most likely to be suitable for exfoliating CrB_2 and MgB_2 .

Solvent Blends. Knowledge of the HSPs of nanomaterials can be used to not only predict the exfoliation efficacy of individual solvents, but also combinations of two solvents. Other researchers have gone on to use these experimentally determined Hansen values for 2D nanomaterials to predict new solvents for successful LPE processing as well as to formulate successful cosolvent blends enabling LPE processing using more mild or low-boiling point solvent mixtures. 33,34 Such solvent blends can vastly improve the flexibility of exfoliating different nanomaterial compositions as they can allow for two solvents with poor exfoliation performance alone to give high concentrations of nanosheets together in certain volume ratios. Since each solvent, solute, and blend of solvents occupies a point in Hansen space, the distance between them, R_a , can be determined by eq 4 below. In principle, the closer two species (e.g., solvent, solute, nanomaterial, etc.) are to each other in Hansen space (i.e., the smaller the R_a), the more likely they are to mix.

$$R_{\rm a} = \sqrt{4(\delta_{\rm D1} - \delta_{\rm D2})^2 + (\delta_{\rm P1} - \delta_{\rm P2})^2 + (\delta_{\rm H1} - \delta_{\rm H2})^2}$$
(4)

To demonstrate an application of HSPs for expanding the list of useable solvents for exfoliating CrB_2 and MgB_2 nanosheets, we used the calculated HSPs of CrB_2 and MgB_2 to predict a solvent blend for each material that can produce higher concentrations of each of the metal diboride nanosheets than either component solvent alone by testing solvent blends with minimum R_3 values with the two metal diborides.

For the solvent blend analysis, we chose solvents that showed both very poor exfoliation efficiency and that were quite far apart in Hansen space from the calculated HSPs for both materials. The solvents were also chosen such that blends would result in a shortening of R_a from the target nanomaterial. For CrB₂, the solvents chosen were MeOH with an R_a of 14.12 and CF with an R_a of 10.00, which led to a minimum R_a of 6.62 near 40% MeOH, as shown in the plot of R_a as a function of solvent ratio (Figure 7a). For MgB₂, the solvents chosen were

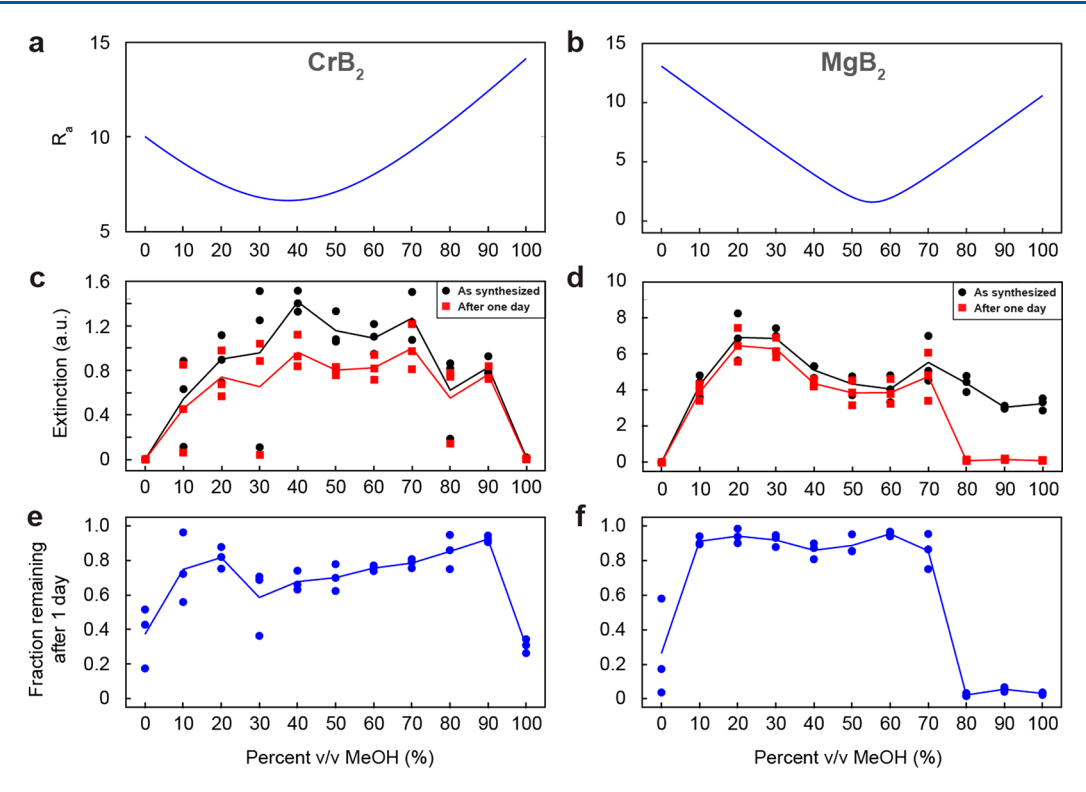


Figure 7. (a) The calculated R_a values for CrB_2 in solvent blends of CF and MeOH. (b) The calculated R_a values for MgB_2 in solvent blends of DCB and MeOH. (c,d) The extinction of CrB_2 (c) and MgB_2 (d) dispersions prepared using various percentages of MeOH in solvent blends with CF and DCB, respectively, after synthesis and after 1 day of sedimentation. (e,f) The fraction of CrB_2 (e) and MgB_2 (f) remaining after 1 day of sedimentation, represented by the fraction of the initial extinction. Solid lines in c-f indicate mean values for three trials of extinction data.

MeOH with an R_a of 10.59 and DCB with an R_a of 13.08, generating a minimal R_a of ~1.6 near 55% MeOH, as shown in Figure 7b.

The metal diboride extinctions for solvent blends in various compositions are shown in Figure 7c,d for measurements taken immediately after exfoliation and the day after. For CrB₂₁ dispersions of CrB2 nanosheets in MeOH or CF alone are consistently poor, showing extinctions of almost zero (Figure 7c). When mixed, however, the combination of solvents allows for dispersions with extinctions of above 1.4 for the 40% MeOH mixture, in agreement with the calculated minimal R_a value. We also observe a general increase in initial MgB₂ nanosheet concentration for the mixtures of MeOH and DCB relative to MeOH or DCB alone. In this case, the maximum concentration occurs with a composition having an R_a with MgB₂ at 8.44 (20% MeOH), which is somewhat far from the expected minimum R_a at ~55% MeOH. Despite this, for both blends, the highest initial concentration is obtained with a composition having a lower R_a with the target metal diboride than either solvent alone.

Furthermore, the initial extinction values for the dispersions from the solvent blends (i.e., CrB₂ in MeOH/CF and MgB₂ in MeOH/DCB) matched or exceeded those for the best individual solvents for these materials determined earlier in the study (i.e., ACN and ACT for CrB₂ and EtOH for MgB₂). The 40% MeOH/CF blend attained an average extinction value for CrB₂ of 1.42 au, almost doubling that of ACN and ACT, having average extinctions of 0.84 and 0.80 au, respectively. Meanwhile, the 20% MeOH/DCB blend produced an MgB₂ dispersion having an extinction value of 6.92 au, exceeding the extinction of the best single-solvent dispersion, MgB₂/EtOH at 6.26 au. These results illustrate that

cosolvent blends can be formulated for CrB_2 and MgB_2 that can exfoliate nanosheets with similar or superior efficiency to ideal individual solvents.

Since the MgB₂ dispersions in pure MeOH were only stable for a few hours before aggregating, we also investigated the stability of the dispersions of MeOH-containing solvent blends the day after synthesis. More detailed stability data for individual solvents were shown in our earlier study. 11 For both CrB2 and MgB2, we found that there is a general increase in stability for the solvent blends compared to dispersions prepared with the constituent solvents alone (Figure 7e-f). For MgB₂ in particular (Figure 7f), we observe that among the compositions we studied, dispersions of MgB₂ that remain stable after 1 day can be produced with compositions comprising 10-70% MeOH, whereas with compositions of 80% MeOH or higher, the dispersions sediment out of solution after 1 day with values close to zero. We also note that some of the dispersions for MgB2 in DCB/MeOH blends within the 10-70% MeOH range remain stable for several days or more.

Comparing the calculated R_a values (Figure 7a,b) to the extinction values for the blends from experiment (Figure 7c,d), we observe a reasonably good correlation between high initial nanosheet concentration and a low R_a in the MeOH/CF system for CrB₂, with the maximum achieved concentration occurring at a composition very close to the minimum value on the R_a curve. For MgB₂, the highly effective solvent compositions occur at 20% to 30% MeOH rather than the 55% MeOH expected from the minimum R_a value. We attribute this difference to uncertainties in the HSP values for MgB₂ and the solvent blends, as well as complexities that may arise in mixtures of polar and nonpolar liquids and their resulting viscosities that are not easily modeled with a simple

equation. Nevertheless, these experiments demonstrate that solvent blends can provide large increases in the concentration and stability for LPE nanomaterials derived from non-vdW solids, and that solvent blends informed by HSP analysis offer a simple and effective way to improve dispersions. The experimental results show that just decreasing the R_a can greatly improve the exfoliation performance, without necessarily finding the optimal concentration with the lowest R_{a} , suggesting, that this is a fairly forgiving phenomenon. Finally, we note that it should be possible to achieve nanosheets of different size and thickness distributions by optimizing the sonication and centrifugation conditions 6,35,36 or by using other size-sorting techniques such as density gradient ultracentrifugation and selective sedimentation³⁷⁻⁴¹ as has been done for other 2D nanomaterials in the literature, although there may be a trade-off between thickness and area, 42 and that the use of solvent blends should provide yet another tool for tuning of the nanosheet distributions from liquid phase exfoliation.

CONCLUSION

We have analyzed the liquid-phase exfoliation effectiveness of two representative metal diboride non-vdW materials, CrB2 and MgB2, using Hansen solubility theory. We found that the viscosity of the solvents must be taken into account when processing the dispersions. Our results showed that nanosheet dispersions with concentrations exceeding 0.02 mg/mL for CrB2 were achieved in ACN and ACT, and 0.5 mg/mL for MgB2 in EtOH. The calculated HSP values for each material can be used to suggest broad classes of solvents that should efficiently exfoliate the two metal diborides, including protic solvents for MgB2 and aprotic polar solvents for CrB2, and help determine the HSP values of solvents most likely to successfully exfoliate each material. The higher $\delta_{\rm P}$ and $\delta_{\rm H}$ values for both materials relative to more traditional vdW nanomaterials suggests additional functionalization with oxy and hydroxy functional groups, and this relationship may likely carry over to other nanomaterials derived from non-vdW solids. We also found that when it is evaluated by its own range of extinction values, CrB2 appears to be successfully exfoliated with a wider range of solvent properties than MgB₂. Such an observation is important for future studies on non-vdWderived nanomaterials, as it suggests that even if a select few solvents do not appear to readily exfoliate a particular material composition in high concentrations, there may be a wide array of solvents that can exfoliate it at least in marginal concentrations, granting more options for processability of non-vdW-derived nanomaterials. The calculated HSPs were then applied toward successful exfoliation of both materials in binary cosolvent blends containing constituent solvents that alone had poor exfoliation effectiveness. We found that at certain compositions of the blends, the initial concentrations of nanosheets either match or exceed those produced by the best pure solvents alone, and exhibit prolonged stability against aggregation. Thus, we have shown the potential applicability of HSPs and solvent blends for the optimization of LPE exfoliation for non-vdW nanomaterials. This study provides a crucial fundamental study of the LPE processing of metal diborides, and will serve as a basis to ignite further research into the solution-phase processing and applications of other non-vdW materials.

ASSOCIATED CONTENT

Supporting Information

The Supporting Information is available free of charge at https://pubs.acs.org/doi/10.1021/acs.langmuir.0c03138.

Detailed information about the optical extinction spectra, extinction coefficients, and size and thickness metrics for selected solvents; average extinction values for each dispersion prepared for calculating the HSPs for both materials; HSPs for the solvents used and nanomaterials; centrifugation times used for each solvent; and details for calculating the weighted standard deviations for the calculated HSPs and the values of weighted standard deviations for both materials under viscosity-corrected conditions (PDF)

AUTHOR INFORMATION

Corresponding Authors

Qing Hua Wang — Materials Science and Engineering, School for Engineering of Matter, Transport and Energy, Arizona State University, Tempe, Arizona 85287, United States;
o orcid.org/0000-0002-7982-7275; Email: qhwang@asu.edu

Alexander A. Green — Biodesign Center for Molecular Design and Biomimetics, The Biodesign Institute and the School of Molecular Sciences, Arizona State University, Tempe, Arizona 85287, United States; Department of Biomedical Engineering, Boston University, Boston, Massachusetts 02215, United States; Email: aagreen@bu.edu

Authors

Matthew S. Gilliam – Biodesign Center for Molecular Design and Biomimetics, The Biodesign Institute and the School of Molecular Sciences, Arizona State University, Tempe, Arizona 85287, United States

Ahmed Yousaf — Biodesign Center for Molecular Design and Biomimetics, The Biodesign Institute and the School of Molecular Sciences, Arizona State University, Tempe, Arizona 85287, United States

Yuqi Guo – Materials Science and Engineering, School for Engineering of Matter, Transport and Energy, Arizona State University, Tempe, Arizona 85287, United States

Duo O. Li — Materials Science and Engineering, School for Engineering of Matter, Transport and Energy, Arizona State University, Tempe, Arizona 85287, United States

AbdulAziz Momenah — Materials Science and Engineering, School for Engineering of Matter, Transport and Energy, Arizona State University, Tempe, Arizona 85287, United States

Complete contact information is available at: https://pubs.acs.org/10.1021/acs.langmuir.0c03138

Author Contributions

M.S.G. and A.Y. contributed equally.

Notes

The authors declare no competing financial interest.

ACKNOWLEDGMENTS

We acknowledge the use of facilities within the Eyring Materials Center at Arizona State University, thank T. Martin and the Metals Environmental and Terrestrial Analytical Laboratory for performing the ICP-MS experiments, and thank Prof. H. Yan for use of his AFM facilities. A.A.G.,

Q.H.W., M.S.G., and A.Y. were supported by NSF grant DMR-1610153. Y.G. and Q.H.W. were supported by NSF grant DMR-1906030. AAG and QHW also acknowledge startup funds from Arizona State University.

REFERENCES

- (1) Coleman, J. N.; Lotya, M.; O'Neill, A.; Bergin, S. D.; King, P. J.; Khan, U.; Young, K.; Gaucher, A.; De, S.; Smith, R. J.; Shvets, I. V.; Arora, S. K.; Stanton, G.; Kim, H. Y.; Lee, K.; Kim, G. T.; Duesberg, G. S.; Hallam, T.; Boland, J. J.; Wang, J. J.; Donegan, J. F.; Grunlan, J. C.; Moriarty, G.; Shmeliov, A.; Nicholls, R. J.; Perkins, J. M.; Grieveson, E. M.; Theuwissen, K.; McComb, D. W.; Nellist, P. D.; Nicolosi, V. Two-Dimensional Nanosheets Produced by Liquid Exfoliation of Layered Materials. *Science* **2011**, 331 (6017), 568–571.
- (2) Kelly, A. G.; Hallam, T.; Backes, C.; Harvey, A.; Esmaeily, A. S.; Godwin, I.; Coelho, J.; Nicolosi, V.; Lauth, J.; Kulkarni, A.; Kinge, S.; Siebbeles, L. D. A.; Duesberg, G. S.; Coleman, J. N. All-Printed Thin-Film Transistors from Networks of Liquid-Exfoliated Nanosheets. *Science* **2017**, *356* (6333), 69–73.
- (3) Ramanathan, T.; Abdala, A. A.; Stankovich, S.; Dikin, D. A.; Herrera-Alonso, M.; Piner, R. D.; Adamson, D. H.; Schniepp, H. C.; Chen, X.; Ruoff, R. S.; Nguyen, S. T.; Aksay, I. A.; Prud'Homme, R. K.; Brinson, L. C. Functionalized Graphene Sheets for Polymer Nanocomposites. *Nat. Nanotechnol.* **2008**, *3* (6), 327–331.
- (4) Gholamvand, Z.; McAteer, D.; Backes, C.; McEvoy, N.; Harvey, A.; Berner, N. C.; Hanlon, D.; Bradley, C.; Godwin, I.; Rovetta, A.; Lyons, M. E. G.; Duesberg, G. S.; Coleman, J. N. Comparison of Liquid Exfoliated Transition Metal Dichalcogenides Reveals MoSe2to Be the Most Effective Hydrogen Evolution Catalyst. *Nanoscale* **2016**, 8 (10), 5737–5749.
- (5) O'Neill, A.; Khan, U.; Coleman, J. N. Preparation of High Concentration Dispersions of Exfoliated MoS 2 with Increased Flake Size. *Chem. Mater.* **2012**, *24* (12), 2414–2421.
- (6) Backes, C.; Szydłowska, B. M.; Harvey, A.; Yuan, S.; Vega-Mayoral, V.; Davies, B. R.; Zhao, P. L.; Hanlon, D.; Santos, E. J. G.; Katsnelson, M. I.; Blau, W. J.; Gadermaier, C.; Coleman, J. N. Production of Highly Monolayer Enriched Dispersions of Liquid-Exfoliated Nanosheets by Liquid Cascade Centrifugation. *ACS Nano* **2016**, *10* (1), 1589–1601.
- (7) O'Neill, A.; Khan, U.; Nirmalraj, P. N.; Boland, J.; Coleman, J. N. Graphene Dispersion and Exfoliation in Low Boiling Point Solvents. *J. Phys. Chem. C* **2011**, *115* (13), 5422–5428.
- (8) Puthirath Balan, A.; Radhakrishnan, S.; Kumar, R.; Neupane, R.; Sinha, S. K.; Deng, L.; De Los Reyes, C. A.; Apte, A.; Rao, B. M.; Paulose, M.; Vajtai, R.; Chu, C. W.; Costin, G.; Martí, A. A.; Varghese, O. K.; Singh, A. K.; Tiwary, C. S.; Anantharaman, M. R.; Ajayan, P. M. A Non-van Der Waals Two-Dimensional Material from Natural Titanium Mineral Ore Ilmenite. *Chem. Mater.* **2018**, 30 (17), 5923–5931.
- (9) Puthirath Balan, A.; Radhakrishnan, S.; Woellner, C. F.; Sinha, S. K.; Deng, L.; Reyes, C. D. L.; Rao, B. M.; Paulose, M.; Neupane, R.; Apte, A.; Kochat, V.; Vajtai, R.; Harutyunyan, A. R.; Chu, C. W.; Costin, G.; Galvao, D. S.; Martí, A. A.; Van Aken, P. A.; Varghese, O. K.; Tiwary, C. S.; Malie Madom Ramaswamy Iyer, A.; Ajayan, P. M. Exfoliation of a Non-van Der Waals Material from Iron Ore Hematite. *Nat. Nanotechnol.* **2018**, *13* (7), 602–609.
- (10) Liu, S.; Xie, L.; Qian, H.; Liu, G.; Zhong, H.; Zeng, H. Facile Preparation of Novel and Active 2D Nanosheets from Non-Layered and Traditionally Non-Exfoliable Earth-Abundant Materials. *J. Mater. Chem. A* **2019**, 7 (25), 15411–15419.
- (11) Yousaf, A.; Gilliam, M. S.; Chang, S. L. Y.; Augustin, M.; Guo, Y.; Tahir, F.; Wang, M.; Schwindt, A.; Chu, X. S.; Li, D. O.; Kale, S.; Debnath, A.; Liu, Y.; Green, M. D.; Santos, E. J. G.; Green, A. A.; Wang, Q. H. Exfoliation of Two-Dimensional Nanosheets of Metal Diborides 2020, 1–32.
- (12) Jun, N.; Norimasa, N.; Takahiro, M.; Yuji, Z.; Jun, A. Superconductivity at 39 K in Magnesium Diboride. *Nature* **2001**, *410* (March), 63–64.

- (13) Fahrenholtz, W. G.; Hilmas, G. E.; Talmy, I. G.; Zaykoski, J. A. Refractory Diborides of Zirconium and Hafnium. *J. Am. Ceram. Soc.* **2007**, *90* (5), 1347–1364.
- (14) Mazánek, V.; Nahdi, H.; Luxa, J.; Sofer, Z.; Pumera, M. Electrochemistry of Layered Metal Diborides. *Nanoscale* **2018**, *10* (24), 11544–11552.
- (15) Li, Q.; Zou, X.; Ai, X.; Chen, H.; Sun, L.; Zou, X. Revealing Activity Trends of Metal Diborides Toward pH-Universal Hydrogen Evolution Electrocatalysts with Pt-Like Activity *Adv. Energy Mater.* 2019 9 (5). DOI: 10.1002/aenm.201803369.
- (16) James, A. L.; Lenka, M.; Pandey, N.; Ojha, A.; Kumar, A.; Saraswat, R.; Thareja, P.; Krishnan, V.; Jasuja, K.; Jasuja, K. Processable Dispersions of Photocatalytically Active Nanosheets Derived from Titanium Diboride: Self Assembly into Hydrogels and Paper-like Macrostructures. *Nanoscale* **2020**, *12* (32), 17121–17131.
- (17) Hansen, C. M Hansen Solubility Parameters: A User's Handbook /. Hansen Solubility Parameters; CRC Press: Boca Raton, FL, 2007.
- (18) Hernandez, Y.; Lotya, M.; Rickard, D.; Bergin, S. D.; Coleman, J. N. Measurement of Multicomponent Solubility Parameters for Graphene Facilitates Solvent Discovery. *Langmuir* **2010**, 26 (5), 3208–3213.
- (19) Cunningham, G.; Lotya, M.; Cucinotta, C. S.; Sanvito, S.; Bergin, S. D.; Menzel, R.; Shaffer, M. S. P.; Coleman, J. N. Solvent Exfoliation of Transition Metal Dichalcogenides: Dispersibility of Exfoliated Nanosheets Varies Only Weakly between Compounds. *ACS Nano* 2012, 6 (4), 3468–3480.
- (20) Patidar, R.; Gunda, H.; Varma, A. K.; Gawas, R.; Das, S. K.; Jasuja, K. Co-Solvent Exfoliation of Layered Titanium Diboride into Few-Layer-Thick Nanosheets. *Ceram. Int.* **2020**, *46* (18), 28324–28331.
- (21) ASTM D7152 Standard Practice for Calculating Viscosity of a Blend of Petroleum Products; Vol. 05.04. DOI: 10.1520/D7152-11R16E01.
- (22) Nečas, D.; Klapetek, P. Gwyddion: An Open-Source Software for SPM Data Analysis. Cent. Eur. J. Phys. 2012, 10 (1), 181–188.
- (23) Gunda, H.; Das, S. K.; Jasuja, K. Simple, Green, and High-Yield Production of Boron-Based Nanostructures with Diverse Morphologies by Dissolution and Recrystallization of Layered Magnesium Diboride Crystals in Water. *ChemPhysChem* **2018**, *19* (7), 880–891.
- (24) James, A. L.; Jasuja, K. Chelation Assisted Exfoliation of Layered Borides towards Synthesizing Boron Based Nanosheets. *RSC Adv.* **2017**, *7* (4), 1905–1914.
- (25) Das, S. K.; Jasuja, K. Chemical Exfoliation of Layered Magnesium Diboride to Yield Functionalized Nanosheets and Nanoaccordions for Potential Flame Retardant Applications. ACS Appl. Nano Mater. 2018, 1 (4), 1612–1622.
- (26) Ogilvie, S. P.; Large, M. J.; O'Mara, M. A.; Lynch, P. J.; Lee, C. L.; King, A. A. K.; Backes, C.; Dalton, A. B. Size Selection of Liquid-Exfoliated 2D Nanosheets 2D Mater. 2019 6 (3). DOI: 10.1088/2053-1583/ab0dc3.
- (27) Nakamura, D.; Nakano, H. Liquid-Phase Exfoliation of Germanane Based on Hansen Solubility Parameters. *Chem. Mater.* **2018**, *30* (15), 5333–5338.
- (28) Nakano, H.; Nakamura, D. Hansen Solubility Parameters of Stacked Silicanes Derived from Porous Silicon. *ACS Omega* **2019**, *4* (7), 11838–11843.
- (29) Yu, W.; Li, H.; Du, N.; Hou, W. Estimation of Surface Free Energy and Solubility Parameters of Mg–Al Layered Double Hydroxides. *J. Colloid Interface Sci.* **2019**, *546*, 361–370.
- (30) Qin, J.; Wang, X.; Jiang, Q.; Cao, M. Optimizing Dispersion, Exfoliation, Synthesis, and Device Fabrication of Inorganic Nanomaterials Using Hansen Solubility Parameters. *ChemPhysChem* **2019**, 20 (9), 1069–1097.
- (31) Tsutsumi, S.; Kondo, K.; Kato, Y.; Fujiwara, N.; Yamamoto, H. Determination of Hansen Solubility Parameters of Particles Using a Capillary Penetration Method. *Chem. Phys.* **2019**, *521* (January), 115–122.

- (32) Chen, X. L.; Tu, Q. Y.; He, M.; Dai, L.; Wu, L. The Bond Ionicity of MB2 (M = Mg, Ti, V, Cr, Mn, Zr, Hf, Ta, Al and Y) *J. Phys.: Condens. Matter* 2001 *13* (29). DOI: 10.1088/0953-8984/13/29/105.
- (33) Zhou, K. G.; Mao, N. N.; Wang, H. X.; Peng, Y.; Zhang, H. L. A Mixed-Solvent Strategy for Efficient Exfoliation of Inorganic Graphene Analogues. *Angew. Chem., Int. Ed.* **2011**, *50* (46), 10839–10842.
- (34) Tasis, D.; Papagelis, K.; Spiliopoulos, P.; Galiotis, C. Efficient Exfoliation of Graphene Sheets in Binary Solvents. *Mater. Lett.* **2013**, 94, 47–50.
- (35) Han, J. T.; Jang, J. I.; Kim, H.; Hwang, J. Y.; Yoo, H. K.; Woo, J. S.; Choi, S.; Kim, H. Y.; Jeong, H. J.; Jeong, S. Y.; Baeg, K. J.; Cho, K.; Lee, G. W. Extremely Efficient Liquid Exfoliation and Dispersion of Layered Materials by Unusual Acoustic Cavitation. *Sci. Rep.* **2015**, *4*, 1–7
- (36) Griffin, A.; Harvey, A.; Cunningham, B.; Scullion, D.; Tian, T.; Shih, C. J.; Gruening, M.; Donegan, J. F.; Santos, E. J. G.; Backes, C.; Coleman, J. N. Spectroscopic Size and Thickness Metrics for Liquid-Exfoliated h -BN. *Chem. Mater.* **2018**, *30* (6), 1998–2005.
- (37) Green, A. A.; Hersam, M. C. Solution Phase Production of Graphene with Controlled Thickness via Density Differentiation. *Nano Lett.* **2009**, *9* (12), 4031–4036.
- (38) Kang, J.; Seo, J. W. T.; Alducin, D.; Ponce, A.; Yacaman, M. J.; Hersam, M. C. Thickness Sorting of Two-Dimensional Transition Metal Dichalcogenides via Copolymer-Assisted Density Gradient Ultracentrifugation. *Nat. Commun.* **2014**, *5* (May), 1–7.
- (39) Zhu, J.; Kang, J.; Kang, J.; Jariwala, D.; Wood, J. D.; Seo, J. W. T.; Chen, K. S.; Marks, T. J.; Hersam, M. C. Solution-Processed Dielectrics Based on Thickness-Sorted Two-Dimensional Hexagonal Boron Nitride Nanosheets. *Nano Lett.* **2015**, *15* (10), 7029–7036.
- (40) Wang, X.; Bai, H.; Shi, G. Size Fractionation of Graphene Oxide Sheets by PH-Assisted Selective Sedimentation. *J. Am. Chem. Soc.* **2011**, 133 (16), 6338–6342.
- (41) Green, A. A.; Hersam, M. C. Emerging Methods for Producing Monodisperse Graphene Dispersions. *J. Phys. Chem. Lett.* **2010**, *1* (2), 544–549.
- (42) Backes, C.; Campi, D.; Szydlowska, B. M; Synnatschke, K.; Ojala, E.; Rashvand, F.; Harvey, A.; Griffin, A.; Sofer, Z.; Marzari, N.; Coleman, J. N; O'Regan, D. D Equipartition of Energy Defines the Size-Thickness Relationship in Liquid-Exfoliated Nanosheets *ACS Nano* 2019. DOI: 10.1021/acsnano.9b02234.